International Journal of Engineering and Environmental Sciences | ***ISSN 1694-4372***
Published by ACADEMIC INK REVIEW | *https://airjournal.org/ijees*
16/18 Avenue des Longaniers, Quatre Bornes, Mauritius
airjournals@gmail.com; enquiry@airjournal.org

Optimization and Characterization of the Casting Conditions of Three Melt Spun Al-Fe-Si-V Ribbons for Elevated Temperatures for Aerospace Applications

Nnamchi, P. S.[1,2] and Zhuo, J.[3]

[1]Department of Engineering Materials, Sheffield University, S13JD Sheffield United Kingdom.
[2]Department of Metallurgical and Metallurgical Engineering, University of Nigeria Nsukka, Nigeria,
[3]Delft University of Technology, The Netherlands

Publication Process	***Date***
Accepted	***April 9th, 2019***
Published	***April 30th, 2019***

ABSTRACT

The microstructural features and mechanical properties of three groups of melt-spun Al-Fe-Si-V ribbons were investigated in order to enhance its optimization for elevated temperature applications and their variation with process variables noted. The influence of cooling rate, heat treatments on the microstructure and mechanical properties are discussed. From the combined studies of microstructure, DSC, XRD and theoretical correlations on the crystallization behaviors of these group of ribbons, it can be concluded that the melt spinning conditions and determines the crystallization behaviors and hence the microstructure. Thus, the characterization results of the three batches of melt-spun corresponding to the flakes produced in 2003, 2004 and 2005, respectively, varied significantly. It was concluded that the melt-spinning conditions were responsible for the variations in the microstructures and mechanical properties of the ribbons.

Keywords: *Casting Conditions; Melt Spun Al-Fe-Si-V Ribbons; Elevated Temperatures; Aerospace Applications*

Introduction

The design of modern aluminum light weight components for automotive engines and aerospace applications require an alloy with high dimensional stability, good wear resistance and adequate room and elevated temperature strengths. The simultaneous requirements of the physical and mechanical properties inevitably lead to the involvement of a number of additives in the alloy, all of which play their own parts in establishing the desired properties. However, the complicated nature of most of the alloy elements makes the conventional ingot casting techniques unsuitable to produce alloys with the necessary, fine dispersion of closely spaced crystals and phases. Therefore, producers have to resort to the technique such as melt spinning (Duwez, 1967; Jones, 1984). Melt spinning as a rapid solidification method has the primary objective of overcoming the limitations associated with conventional material solidification processing. To date, one of the most successful techniques to manufacture dispersion-strengthened alloys has been melt spinning, where a molten metal is rapidly solidified by systematic contact with a rotating heat sink. A very high cooling rate realized in the process is paramount to the formation of the required dispersoids on a fine scale. Since the inventions of melt spinning by Pol Duwez in the early part of this century, the use of melt spun aluminum alloy has been extensive in automotive and aerospace applications. However, recent studies have shown that the microstructure and mechanical properties of this alloy have become less desirable, due to variations in melt-spinning and subsequent processing conditions (Duwez, 1967; Cantor, 1994).

The metallurgical properties of rapidly quenched Al-transition-metal alloys containing Fe have been studied over the years such as the review by Jones, (1978), Thuishield, & Stowell, (1974). Among, all these alloys, Al-Fe-V-Si has shown the best combinations of room-temperature and elevated-temperature mechanical properties, which makes this alloy quite attractive and suitable for applications at elevated temperatures up to 400°C. The alloys produced possess good elevated-temperature properties that are comparable with those of Ti alloys on a specific strength basis, when the melt spinning conditions are right (Skinner, Bye, Raybould & Brown, 1986; Peng, Zhu, Wang, Chen, Ma & Bi, 1999; Skinner, 1988). The elevated-temperature properties of this alloy are driven by the presence of alloy elements like Fe and Si, which have low solid solubility limit in aluminum, and high liquid solubility to allow a large volume fraction of dispersoids to form in the microstructure after rapid solidification. The microstructure of this alloy is sure to be thermally stable and could be attributed to the low diffusivity of the dispersoids formed, which will ensure minimal coarsening rate during high temperature exposures (Rodriguez and Skinner, 1990; Cantor, 1994). Therefore, the alloy will maintain the strength and toughness up to a high fraction of the alloys melting temperature.

The present investigation is part of systematic industrial study of the process optimization for enhanced mechanical properties at elevated temperatures on three batches of melt spun Al-Fe-Si-V ribbon for aerospace applications. These ribbons have shown some structural inhomogeneities and variation in mechanical properties, though on a microscale within the finished products made from these ribbons. Obviously, studying the variations in the structure and the mechanical properties of the various batches of the ribbons will enable us determine, if the melt spinning operations have changed over the years or not.

Table 1: Composition determined by wet chemical analysis test and XRD (approx. inst. error of ±0. 5% for the XRD)

Samples	Al(at.%)	Fe(at.%)	V(at.%)	Si(at.%)	Fe (at.%)by XRD
Flake A	balance	8.77	1.27	0.31	8.75
Flake B	balance	8.66	1.28	0.51	8.34
Flake C	balance	8.43	1.35	1.08	8.17

Experimental Procedure

The raw material in the form of the three batches of ribbons that was used for this investigation were produced using similar conditions and alloying elements, supplied by RSP Technology in the Netherlands. As the metallic ribbons were produced in different years, in this work, they are coded as *A* for the ribbons produced in year 2003, *B*

for the ribbons produced in year 2004, *C* for the ribbons produced in year 2005.

Wet chemical analyses and X-ray diffraction shown in Table 1, were the two approaches used to determine the actual compositions of the alloys. Wet chemical analysis by flame atomic absorption spectroscopy (FAAS) requires a liquid or dissolved sample to be aspirated, aerosolized and mixed with combustible gases, such as acetylene and air or acetylene and nitrous oxide. The mixture is ignited in a flame whose temperature ranges from 2100 to 2800 °C. During combustion, the atoms of the element of interest in the sample are reduced to free, unexcited ground state atoms, which absorb light at characteristic wavelengths. The characteristic wavelengths of this technique are element specific to the accuracy of 0.01 - 0.1 nm. To provide element specific wavelengths, a light beam from a lamp whose cathode is made of the element being determined is passed through the flame. A device such as photon multiplier can detect the amount of reduction of the light intensity due to absorption by the analyte, and this can be directly related to the amount of the element in the sample. X-ray diffraction approach is based on earlier report and data compared from literatures showing that an estimate of the stoichiometry of the quasicrystalline phase in rapidly quenched Al-transition-metal alloys can be obtained from the relative amplitude of the quasicrystalline peaks and the FCC Al peaks observed in the X-ray diffraction patterns using Eqn.1 according to Jones (1983). The changes in the lattice parameter of the α-Al phase with respect to the ideal crystal lattice of a pure aluminum matrix were quantitative measured.

$$X_{XRD} = \frac{0.4050 - \alpha}{0.00072} \quad \text{.....(1)}$$

Where χ is the composition of Fe expressed in atomic percent (at. %), and the α is the lattice parameter in nanometer, used to determine the composition of the alloy. Lattice parameter measurements were made using a high purity Si monochrometer that had a {511} orientation as a standard on X-ray diffractometer with Co-Kα radiation. This {511} orientation had no reflection and therefore would not interfere with the reflections from the sample. This is because copper reflections would cause a fluorescence effect in the present alloy containing iron as one of its major alloying element leading to high background noise, while cobalt tended to reduce this background noise. X-ray analyses of this alloy with a density of 2.92 g/mm3 showed by the calculated absorption (photoelectric + Compton's effect + Rayleigh) that 90% of the diffracted beam would contribute to a 37.68μm penetration depth in the sample.

Previous result in melt spinning on the development of microstructure in advanced solidification processing had shown that low cooling velocity could occur as a result of an increasing heat conduction distance between solidifying melt and heat sink (Cantor, 1994). This is mainly, because during melt spinning the cooling conditions is near Newtonian and therefore the ribbon temperature will decrease exponentially with time according to Eqn.2 (Boswell & Chadwick, 1977).

$$T - T_W = (T_i - T_W)\exp\left(-ht/X_{\rho C}\right) \quad \text{..... (2)}$$

Where T_W and T_i are the wheel and initial melt temperature of 278 and 1223K, respectively, *h* the heat transfer coefficient (6×10^5 W/m2K) at the ribbon/wheel interface, *X* the ribbon thickness, the melt density (2.92 g/cm^3), ρ and the specific heat for the ribbons $C\rho$ = *100* J/kgK. Over a small solidification temperature range, the equation is approximately linear and the mean cooling rate $\frac{dT}{dt}$ calculated using Eqn. 3 (Skinner, Bye, Raybould, & Brown, 1986; Boswell, & Chadwick, 1977).

$$\frac{dT}{dt} = h(T_t - T_w)X_{\rho C} \quad \text{..... (3)}$$

Reports by Bendijk, Delhez, Katgerman, De Keijser, Mittemeijer &
van der Pers, (1980); Kirin, Tonejc & Bonefa, (1969) for any given rapid-quenching technique show that the thickness

of a ribbon is indicative of the average cooling rate, provided that the experimental conditions are reasonably constant. The means that higher cooling rate would translate to thinner the ribbon as well as larger concentrations of elements (Fe, Si) in the solid solution. In line with those investigations, a direct correlation for the cooling rate was made from the ribbon thicknesses and the dendrite arm spacing using Eqn. 4 is shown in Table 2 according to Boswell and Chadwick, (1977)

$$\lambda = \beta \varepsilon^{-n} \quad \text{..... (4)}$$

Where λ = spacing/cell arm space size, ε = cooling rate (K/s); β = 50μm $(Ks^{-1})^{1/3}$, and the constant *n* = 0.3. This equation implies that the thickness of the ribbons is related to the achievable interface velocities and the rate of heat extraction by the substrate. The two factors can limit undercooling obtained in melt spinning by reducing the heat transfer, thereby controlling the microstructure development.

The microstructure of the flakes was examined by using an optical microscope to monitor the changes that occurred during the processing of the sample. The microscopic observations were performed using a Neophot 2" optical microscope. Images were recorded with a Nicon DXM 1200 camera attached to the microscope and evaluated using an Aquinto software image-processing program. The Stanton Redcroft 1200 DSC instrument was used to study the phase transformations, precipitation reactions and the stability of the flakes by heating (scanning) a 0.012 g sample at a constant rate of 20 °C per min from 200 to 800 °C. At this temperature, the material was held isothermally for 5 min before cooling.

The influence of annealing on the microhardness of the flakes were evaluated as a measure of the mechanical strength from room temperature to 450 °C for 1 hour. This was done in other to determine the dispersion hardening response of the ribbons to Vickers microhardness. During the measurement, untypical low values were rejected on the assumption that sub-surface defects were responsible. Therefore, the measurements excluded the areas where normal melt spinning defects, particularly porosity are present. This microhardness result may be extended to give an indication of the tensile strength of this RSP AA809 aluminum alloy. Experimentally, Since $\mathrm{H}\nu = \delta_y / 3$, where δ_y and HV are the yield stress and Vickers microhardness respectively, therefore these values can be compared with the 0.2% strength of aluminum.

Table 2: The values of lattice para., thickness as well as the calculated cooling rates based on Eqn. (2), (3) and (4)

Samples	Lat. Par.(A°)	FWHM(2=Theta	Thickness(μm)	Cooling rate(K/sec)
Flake A	4.0483	0.706	35.41	5.2×10^6
Flake B	4.0468	0.656	87.71	2.28×10^5
Flake C	4.047	0.616	89.08	2.14×10^5

Result and Discussion

The experimental determined composition results for the three alloys (all in atomic %) by wet chemical and X-ray diffraction analyses to estimate the solubility of Fe, along with the cooling rates calculated from the ribbon thickness using Eqs. (1) (2), (3) and (4) are given in Table (1) and (2)
respectively. Table (1) is comparing the composition using calculated composition of Fe using XRD and experimental measured composition analyses for the three batches of the alloys. It can be seen that both methods of calculating theoretically the concentration of Fe yielded values that are very close to the measured ones. An additive importance of using Eqn. (1) is that it is simpler, quicker and can be used in a predictive fashion. This indicates not only that using the lattice parameter equation can accurately estimate the exact composition of Fe in this alloy according to Skinner, (1988), but also that the actual composition of the alloys or ribbons varied within the three years of production. Indeed, this may not only have varied the quality of the flakes, but also the mechanical properties of the extruded

billets produce from the flakes.

The result comparing the thickness of the flakes and the calculated cooling rates used during the melt spinning of the samples given in Table (2) are quite interesting in several aspects concerning the fundamental reasons behind the variations in composition and other characteristic features of the flakes. Our measurements show a consistent decrease in lattice parameter as a function of Fe content and cooling rates, this is in line with results presented earlier (Cantor, 1994; Skinner, 1988; Mittemeijer, & Delhez, 1978). The calculated lattice parameter of the aluminum matrix decreased from 0.4525 to 0.40519 nm from ribbon A to ribbon C. Therefore, if the influence of X-ray diffractometer (which was set at identical condition) on the accuracy of the measurements is left out of consideration, the variation can be ascribed to the resolution of the alloying elements in the aluminum matrix. And since most metastable phases in this alloy form at a much higher concentrations of Fe, some of the Fe would preferentially dissolve into other equilibrium phases causing the quantity of Fe dissolved in the αAl phase to decrease in effect of the low cooling rate used. This is consistent with what several authors have reported about solubility of Fe in rapidly quenched Al of about 6at. % (Jones, 1978; Humphrey, Warren, Titchmarsh & Cerezo, 2001).

Figs. (1), (2) and (3), show the microstructures of the three groups of ribbons A, B and C respectively. Tables 1 and 2 compares the variations in the microstructures as a function of cooling rate and composition. Since the cooling rate during rapid solidification increases with decreasing grain size, one can infer that the crystallization increases process in ribbon A group has been better suppressed due to the high cooling rate and large undercooling. The comparisons show that the ribbons produced in year A possessed a high volume of Fe and the best cooling rate. The microstructure is made up of 90% of zone A (amorphous phase), According to Table 2, the lattice parameter of the αAl phase in the ribbons varied from 0.40483 nm in ribbon A to 0.4047 in group C ribbons. All the values are however large than that of the as cast material of 0.4055nm; confirming that the lattice parameter has increased with increasing solidification rate, due to supersaturation of Al with solute elements. Realizing that the atomic radius of Si is smaller than that of Al, apart from V which act to refine the grain, the increase in lattice parameter of αAl phase seem to be related to the presence of large amount of Fe in the αAl phase of the rapidly solidified ribbons than under equilibrium conditions. The composition of the Fe in the ribbons would certainly be a reflection of the rapid solidification conditions.

Other significant features observed in the flake B and C included (i) very little Zone *A* microstructures and (ii) several equiaxed dendrites commonly observed in the Zone B microstructure with a range between 3.0 - 3.5µ*m*. Figs. (2b) and (3b) shows a magnified image of the zone B microstructure of flake B and C respectively. The presence of the dendrites in these microstructures was an indication of a lower solidification rate applied during the melt-spinning operation. In general, the present study interestingly, but contrary to popular views and reports shows that the coarser microstructure (Zone B) can also be formed almost on the wheel side. The results show that the thickness in each of the zones depends on the melt-spinning conditions. This dendritic condition could arise when a small perturbation at the interface ended up in even more supercooled liquid so the interface became unstable in several directions (Birol & Karlik, 1996). This type of dendrite growth was a frequently observed growth mode in conventional aluminum casting and welding processes, where cooling rate was less rapid (Bhadeshia). Variable cooling rates might have been the main indicator accounting for the unusual variations of microstructures observed in these flakes.

Figs. 4 shows the DSC traces of the three groups of ribbons. Here we find that the number of exothermic peaks is different in the different ribbons. One peak in ribbon C and two clear peaks one at 680.5ºC and the other 730 - 800.8 ºC can be seen from group A and B. The second exothermic peak was of very low intensity and barely visible, but about the same temperature in ribbon A and B. Thus, we can conclude that the ribbons that have solidified most rapidly showed two exothermic peaks (ribbons A and B), while those that solidified relatively slowly showed only one exothermic peak (ribbon C). It can be concluded from the XRD profile that the first exothermic peak (at 680.5ºC) was due to the precipitation of the αAl phase from the amorphous zone A phase while the second peak (at730 - 800.8 ºC) was due to the precipitating intermetallics, such as Al_6Fe_6, $Al_{11}V$, FeAl phases. Since the precipitating

intermetallics have very similar characteristics (both structure and lattice parameter), it is only natural to expect that many of them will precipitate out at about the same temperature, thus explaining the broad nature of the second peak. The DSC traces presented in Fig. 4 can be interpreted in the following way. The observation of the two peaks in A and B suggest that the ribbons contain mostly the amorphous zone A phase as shown from their micrographs (perhaps with some amount of the αAI phase as indicated by the XRD patterns).

Figs. 6 shows the distribution of the microhardness measured along the cross-sectional surface of the flakes, while Fig. 5 is a measure of the Vickers microhardness in ribbon C as a measure of the mechanical property in the three groups of ribbons. The alloy produced in 2003 (ribbon A), which has a high microhardness, can be due to quenched in dispersoids. The variation noted from microhardness along the surface of the ribbon is consistent with the inhomogeneous microstructures. A reasonably high microhardness was observed in ribbon A. This would translate to applying high extrusion pressure during extrusion, by the quenched in dispersoids acting as dislocation barrier. The results about anneal temperatures on the flake produced in sample C, shows that the yield strength of this particular ribbons and/ or its finished product would be within 300 ºC - 400 ºC. This entails that the material might be used above this temperature range due to coarsening that might appear on the initial microstructure and dissolution of the dispersed crystals into the matrix. This result will be very useful in estimating the exact extrusion window and the service temperature during applications.

Conclusions

From the combined studies of microstructure, DSC, XRD and theoretical correlations on the crystallization behaviors of these group of ribbons, it can be concluded that the melt spinning conditions and determines the crystallization behaviors and hence the microstructure. Thus, characterization results of the three batches of melt-spun Al-Fe-V-Si ribbons A, B and C show that the samples produced in 2003, 2004 and 2005, respectively varied significantly. Sample A consisted of the amorphous (feature-less Zone A) and microcrystalline (Zone B) microstructures in a ratio of 40 to 60, while B and C consisted predominantly of the coarser microcrystalline (highly dendritic) Zone B microstructure. The variation in the as-melt-spun microstructure was considered to be due to variations in solidification rate.

The correlation analyses between the flake thicknesses, dendrites arm spacing and the cooling rate used during the melt-spinning operations decreased as the cooling rate decreased from 5.2×10^{6} to 2.14×10^{5}Ksec^{-1}. These variations in cooling rate were strongly dependent upon variations in melt-spinning conditions. Microhardness show that coarsening of the microstructure, dissolution of the dispersed crystals into the matrix occurred after annealing treatments at 400 ºC for 1. The implication might be that the ribbons would not be suitable to produce alloys used for elevated-temperature applications above the temperature range.

References

Bendijk, A., Delhez, R., Katgerman, L., De Keijser, Th. H., Mittemeijer, E. J. and Van Der Pers, N. M. (1980). Characterization of Al-Si-alloys rapidly quenched from melt. *Mat. Sci. & Eng.,* 15, 2803-2810.

Bhadeshia, H. K. D. H. http://www.msm.cam.ac.uk/phase-trans/abstracts

Birol, Y. and Karlik, M. (1996). Microstructure of a thin-cast Al-Fe-Mn-Si strip. *Mat. Sci. & Eng.,* 31, 2139-2143

Boswell, P. G. and Chadwick, G. (1977). The grain size of splat quenched alloys. *Scri. Met.,* 2, 459-465

Cantor, B. (1994). Development of microstructure in advanced solidification processing. *Micron*, 25, 551-556

Dunlap, R. (1985). Formation, structure, and crystallization of metastable quasicrystalline Al-transition metal alloys prepared by rapid solidification. *Can. J. Phys.,* 63, 267-282.

Duwez, P. (1967). Rapidly chilled amorphous alloy films. *Trans. Am. Soc. Metals*, 60, 607-626.

Humphrey, E. S., Warren, P. J., Titchmarsh, J. M. and Cerezo, A. (2001). Microstructure and chemistry of Al–V–Fe–Si nanoquasicrystalline alloys. *Mat. Sci. & Eng. A,* 304, 844-848.

Inoue, A. (1998). Amorphous, nanoquasicrystalline and nanocrystalline alloys in Albased Systems, Prog. *Mat. Sci.,* 43, 365-520

Jones, H. (1978). Aluminum., 54, 274.

Jones, H. (1983). On the prediction of lattice parameter vs. concentration for solid solutions extended by rapid quenching from the melt. *Scripta Mater.,* 17, 97-100.

Jones, H. (1984). Microstructure of rapidly solidified materials. *Mat. Sci. & Eng.*, 19, 1043-1056

Kirin, A., Tonejc, A., and Bonefa, A. (1969). Change in the lattice parameter of aluminum under the influence of rapid quenching from the liquid state. *Scr. Met. & Mat.,* 3, 943-946.

Mittemeijer, E. J. and Delhez, R. (1978). Concentration variations within small crystallites studied by x-ray diffraction line profile analysis. *J. Appl. Phys.,* 49, 3875-3879

Peng, L. M., Zhu, S. J., Wang, F. G., Chen, H. R., Ma, Z. Y. and Bi, J. (1999). High temperature creep deformation of an Al–Fe–V–Si Alloy. *Mat. Sci. & Eng. A*, 259, 25-33.

Rodriguez, M. A. and Skinner, D. J. (1990). Compositional analysis of the cubic silicide intermetallics in dispersion strengthened Al-Fe-V-Si alloys. *Mat. Sci. Let.,* 9, 1292-1293.

Skinner, D. J. (1988). Physical metallurgy of dispersion strengthened Al-Fe-V-Si alloys in Dispersion Strengthened Aluminum Alloys, Mineral, Metals and Material Society Annual meeting, Warrendale. PA, 437-450.

Skinner, D. J., Bye, R. L., Raybould, D. and Brown, A. M. (1986). Dispersion strengthened Al-Fe-V-Si alloys. *Scr. Met.,* 20, 867-872

Sobolev, S. L. (1997). Rapid solidification under nonequilibrium conditions. *Physical Rev. E*, 55-6, 6845 -6854.

Thuishield, G. and Stowell, M. J. (1974). Mechanical properties of Al-8wt%Fe –based alloys prepared by rapid quenching from liquid state, *Mat. & Eng.,* 9, 1644-1660

APPENDIX I

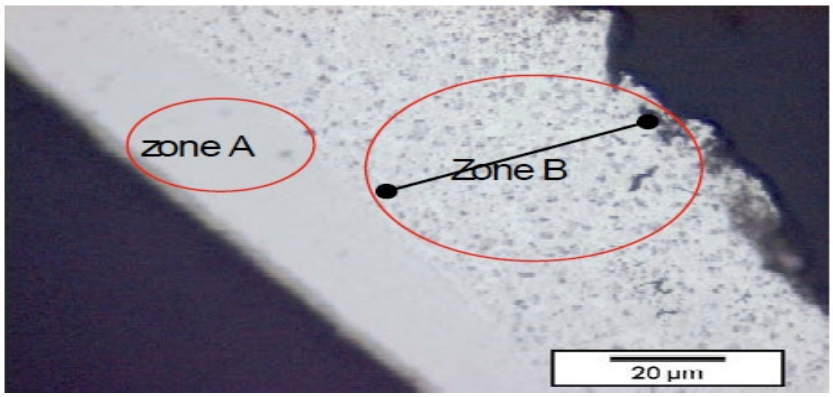

Fig.1: Optical micrograph of etched flake A showing the presence of Zone A and Zone B surrounded by relatively spherical dispersoids

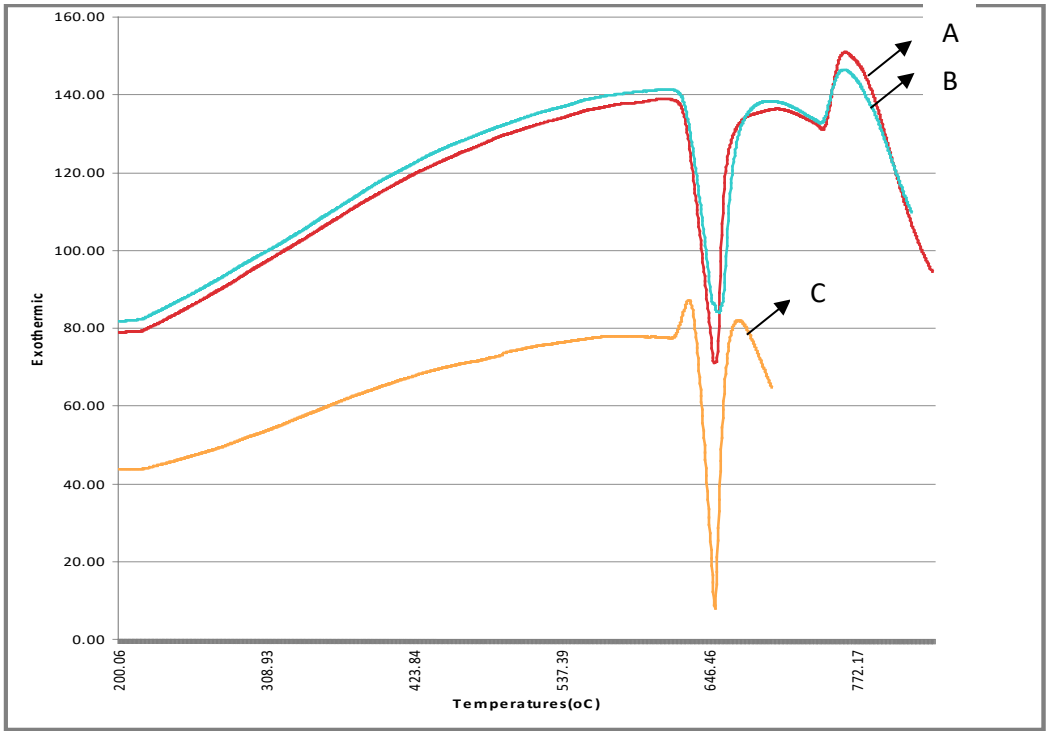

Fig.2: (a) Optical micrograph of etched flake B showing a limited area of Zone A as well as the dendrite structures existing within Zone B and (b) a high magnification micrograph of Zone B.

APPENDIX II

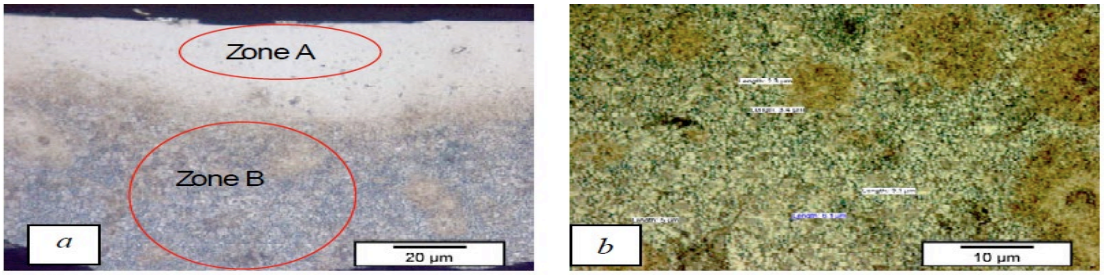

Fig.3: (a) Optical micrograph of etched C showing a limited Zone A structure as well as equiaxed dendrite structures within Zone B and (b) a high magnification micrograph of Zone B

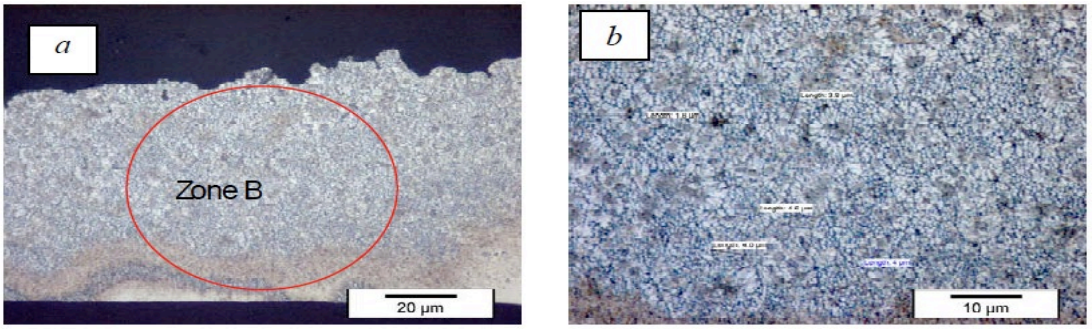

Fig. 4: DSC traces for the three groups of ribbons with grain sizes (A)> 45µm, (B) 50-60µm and (C) above 70µm

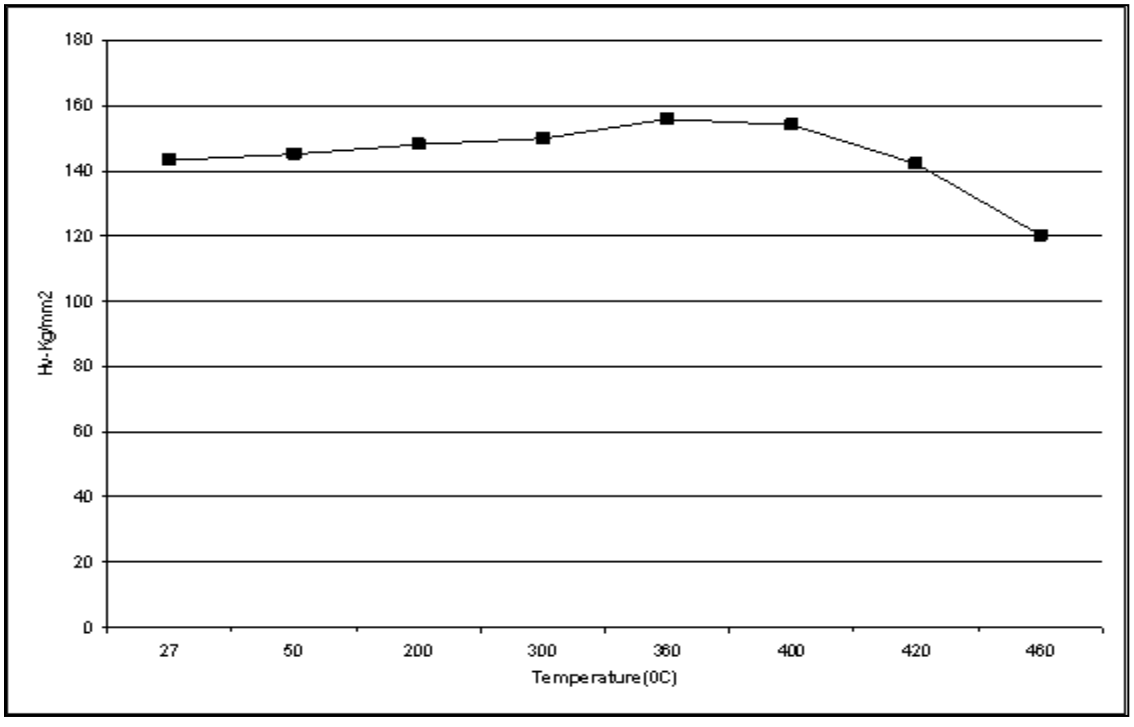

Fig. 5: Vickers microhardness values across the surface of the ribbons

APPENDIX III

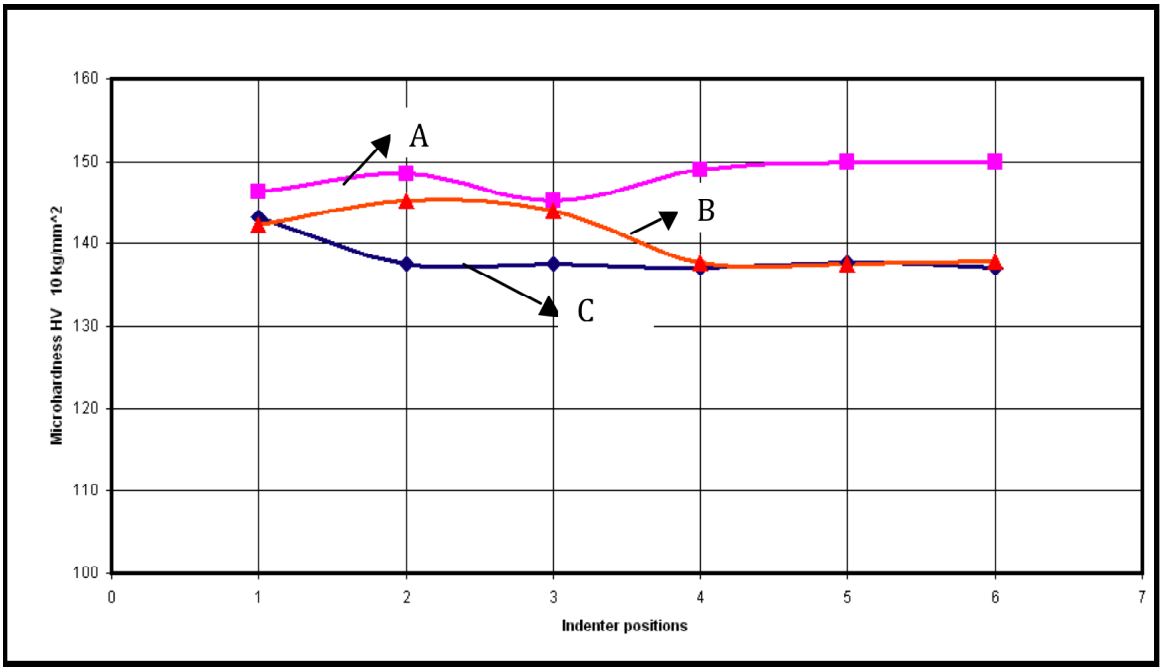

Fig. 6: Influence of temperatures on the microhardness of group C ribbons